Charge and spin transport in Nb-doped SrTiO3 using Co/AlOx spin injection contacts

Kamerbeek, Alexander

Chapter 6

Coexistence of electro-resistance and tunneling anisotropic magneto-resistance in Co/Nb:$SrTiO_3$ devices at room temperature

Abstract

We show the co-existence of both tunneling anisotropic magneto-resistance (TAMR) and resistive switching at room temperature in Co/Nb:$SrTiO_3$ diodes with and without a thin insulating AlO_x layer at the interface. The room temperature TAMR displays an unconventional bias dependence leading to a maximum TAMR of 1.7 % at a relatively large reverse bias of −75 mV. This is significantly higher than the room temperature TAMR effect size of around 0.3 % reported for junctions using conventional semiconductors. The unconventional behavior as well as the large amplitude of the TAMR effect is attributed to the large permittivity of Nb:$SrTiO_3$. Additionally, large electro-resistive switching is observed with an on/off ratio around 80 at low bias readout voltages. The simultaneous existence of both TAMR and electro-resistance holds promise for realizing both charge and spin based memory in a single device.

A.M. Kamerbeek et al.
in preparation.

6.1 Introduction

The realization of data storage or logical operations where not only the electron charge but also its spin is utilized is referred to as spintronics. A major landmark in spintronics is the discovery of Giant (GMR) and Tunneling Magneto-Resistance (TMR) which resulted in an incredible increase in the data storage capacity of hard-disk drives. There is also an active field of research on TMR based devices to realize magnetic random access memory which are currently becoming available on the market. The MR effect in these devices is realized by switching the relative magnetization direction of two ferromagnetic layers separated by a conducting metal (GMR) or insulating tunnel barrier (TMR). This is shown in Fig. 6.1(a) and (b) where the white arrows represent the magnetization direction and the black arrows the current density through the junction. Therefore the device structure needed to realize GMR or TMR sensors is relatively complex. This is due to the tendency of magnetic layers in close proximity to couple and the difficulty of maintaining spin coherence between the two magnetic layers.

More recently it has been observed that the resistance of such MTJs can also be altered by rotating the ferromagnets magnetization with respect to its crystallographic axes or the current flow direction. This effect is referred to as Tunneling Anisotropic Magneto-Resistance (TAMR). Remarkably, the TAMR effect is also observed when one of the ferromagnet layers is replaced by a non-magnetic material (see Fig. 6.1(c)). This is a significant advantage over the TMR effect as it not only reduces the device complexity but allows the counter electrode to be, for instance, a semiconductor. Although very large TAMR effects have been observed for (Ga,Mn)As [10] and antiferromagnetic IrMn [11] based junctions they only work at very low temperatures ($\leqslant$ 4.2K). When conventional transition metal ferromagnets are used (e.g. Co, Fe or Mn),

Table 6.1: TAMR effect sizes for transition metal ferromagnets

FM	Barrier	TAMR type	Temperature	TAMR size	Ref.
CoFeB	MgO	oop	300K	0.3 %	[1]
Fe (epi)	Schottky n-GaAs	ip and oop	300K	0.3 %	[2]
IrMn	AlO_x	ip and oop	300K	0.24 %	[3]
Co	AlO_x	ip	125K	0.8 %	[4]
Co	AlO_x	oop	100K	0.06 %	[5]
Fe (epi)	GaAs	ip	100K	0.3 %	[6]
CoFe	MgO or AlO_x	oop	10K	0.5 %	[7]
Co (epi)	AlO_x	ip	5K	11 %	[8]
CoFe	Schottky n-GaAs	ip	4.2K	0.5 %	[9]

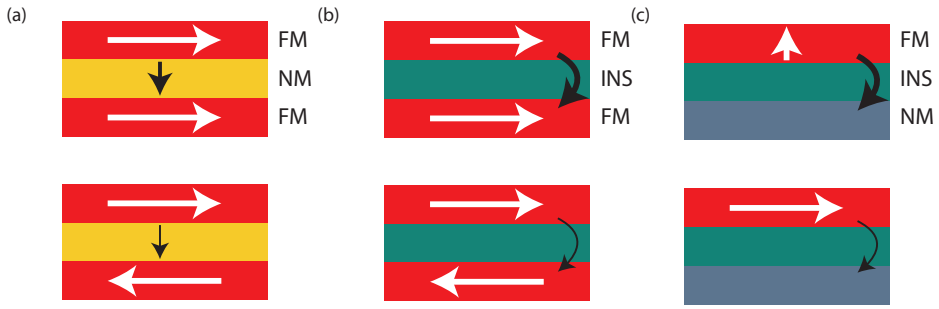

Figure 6.1: (a) Heterostructure of a ferromagnet(FM)/normal metal/ferromagnet junction for the giant magneto-resistance effect. The junction resistance is larger when the magnetization of the FM's is anti-parallel (b) Similar as in (a) but the normal metal is replaced by an insulator resulting in the tunneling magneto-resistance effect. (c) By rotating the magnetization of the FM its (surface) electron density of state is changed which alters the tunnel conductance through the junction. Such a heterostructure requires only a single FM electrode and the effect is known as tunneling anisotropic magneto-resistance

room temperature TAMR is observed but generally amounts to only a fraction of a percent [1–3]. For instance, in a report employing a Co/AlO_x/Pt junction a TAMR size of 0.06 % was observed up to 100 K. In table 6.1 an overview of TAMR sizes with transition metal ferromagnets in published literature is given as well as the material system used, oop stands for out-of-plane and ip for in-plane.

In this work we show TAMR values as large as 1.7 % at room temperature at a relatively high bias of around −75 mV using Co/Nb:$SrTiO_3$ Schottky junctions. A strongly asymmetric decay of the TAMR size with bias is observed. Both the large enhancement of the TAMR size and the asymmetric decay are explained by the very large permittivity of $SrTiO_3$ which causes a much larger electric field at the surface of the Co layer compared to conventional semiconductors such as Si or GaAs.

Apart from the demonstration of large TAMR effects, it is well known that metal/n-$SrTiO_3$ interfaces exhibit electro-resistance [12–18]. This allows changing the charge resistance of the Schottky interface at low operating voltage by cycling it to high negative or positive voltage. Effectively this produces a memory resistor where the resistance state is retained without supplying any power (i.e. a non-volatile memory). Furthermore the resistance state can be be set to an arbitrary value, within a certain window, and is determined by the history of the voltage bias of the device. Additional advantages of a Schottky based resistive memory are its ease of fabrication and scaling of its dimensions. Furthermore, no forming step is needed to realize initial operation of the system unlike, for instance, filament based M/I/M devices [19].

The devices in this chapter exhibit, apart from a large room temperature TAMR, an electro-resistive effect allowing an on/off ratio of around 80 at low bias. Further-

more, by selecting the maximum set or reset bias the low voltage resistance can be tuned. As the TAMR magnitude is fully controlled by the junction voltage the resistive switching of the devices does not impede the TAMR effect. Generally the magnetoresistance is significantly deteriorated when restively switching the junction, for instance in spin memristive tunnel junctions. Therefore, using non-magnetic Nb:$SrTiO_3$ as the counter electrode to Co shows potential for realizing devices with simultaneous spin and charge based memory functions.

6.2 Experiment

To investigate the TAMR and electro-resistive switching a three terminal (4-probe) measurement geometry is employed as shown in Fig. 6.2. This geometry ensures only the contact resistance of the central junction is probed, eliminating any series resistance from the leads or the semiconductor bulk. To measure the electro-resistance a dc two-probe voltage is sourced and the associated two-probe current and four-probe voltage are measured to obtain the *I-V* characteristics as shown on the left side of Fig. 6.2. The typical electro-resistive character of the device is shown in the graph below. The junction is initially in a low resistance state (LRS, R_{base}) which was set by applying a positive voltage of around 400 mV. When sweeping to −1.5 V (black curve) and back to zero (red curve) the junction is in a high resistance state (HRS, R_1) with a ratio of $R_1/R_{base} \sim 3$. The junction is reset to the LRS by applying 400 mV and is now swept to −3 V, reset again and swept to −6 V. Compared to the −1.5 V sweep an increasingly higher resistance state is obtained with a maximum ratio of $R_3/R_{base} \sim 120$ around −1 V.

To measure the TAMR a constant dc current is sourced and the four-probe voltage is measured as function of the out-of-plane applied magnetic field as shown in the right side of Fig. 6.2. When the magnetic field is increased the magnetization of the cobalt layer (M) is rotated out-of-plane with angle θ. A typical room temperature MR response of the junctions is shown in the graph below. The lineshape is almost parabolic with a slight deviation at large fields due to a small misalignment of the magnetic field with the surface normal. At a junction voltage of −75 mV a voltage change with magnetic field of almost 1.2 mV is observed which amounts to an MR of 1.6%.

6.2.1 Tunneling Anisotropic Magneto-Resistance measurements

In Fig. 6.3(a) and (b) a selection of TAMR measurements is shown for varying positive and negative current biases, respectively. A clear parabolic dependence of the junction voltage is observed as function of the magnetic field, as is expected due to the shape anisotropy of the thin film ferromagnet. For positive bias a clear scaling of

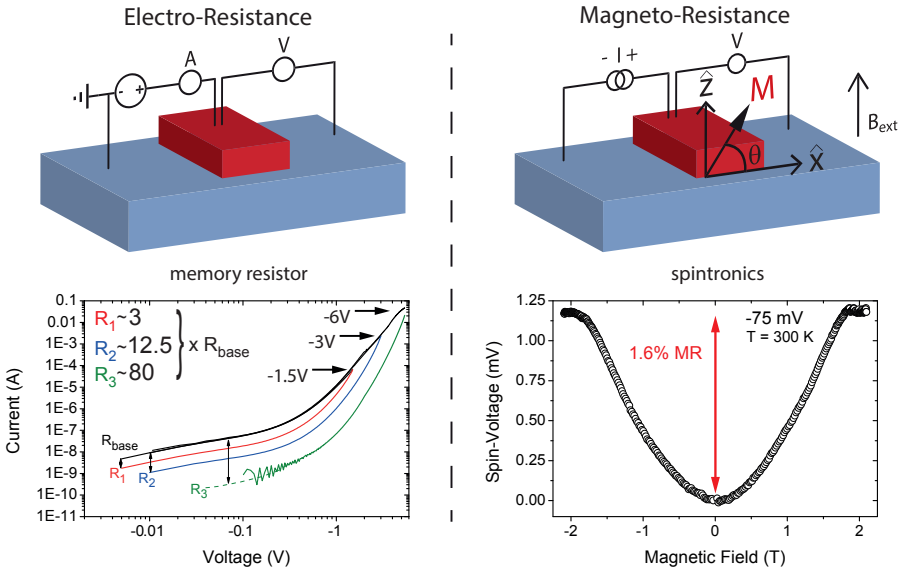

Figure 6.2: Coexistence of resistive switching and TAMR in Co/Nb:$SrTiO_3$ junctions. (left side) Measurement geometry for electro-resistance characterization. Below a set of negative bias sweeps showing that the low bias resistance can be set to an arbitrary value below R_{base} depending on the maximum negative voltage of the sweep. Between each sweep the device is reset to R_{base} by sweeping to 400 mV. (right side) Measurement geometry for TAMR characterization. A clear parabolic TAMR effect is observed as shown in the bottom figure with an amplitude of 1.6 % at −75 mV.

the TAMR amplitude with current bias is observed up to roughly 50 nA after which the amplitude stays constant. A measurement with zero bias is also shown (solid black line) showing no junction response out of noise. At a very large bias of 20 mA the amplitude is seen to decrease slightly. This saturation is not observed at negative bias where an increase in the TAMR amplitude is observed up to at least −1 mA. The dashed black lines are fits using $\Delta V \sin^2(\theta)$ with theta the angle as defined in Fig. 6.2. At very large positive and negative currents a small deviation of the lineshape is observed when the field crosses zero. This might originate from a very small AMR effect in the cobalt layer since the Schottky resistance becomes very low in the high bias region.

The amplitude of the TAMR effect, defined as $V(\theta = 0°) - V(\theta = 90°)$, is plotted versus positive and negative junction voltage in Fig. 6.4(a) and (b), respectively. The amplitude shows a very rapid scaling at small voltage bias for both polarities. At ∼50 mV the amplitude saturates and shows a slight decay above 400 mV. At negative bias a linear relation between junction voltage and TAMR amplitude is observed up to at least 5.5 V. Such a roughly linear relation between junction voltage and TAMR

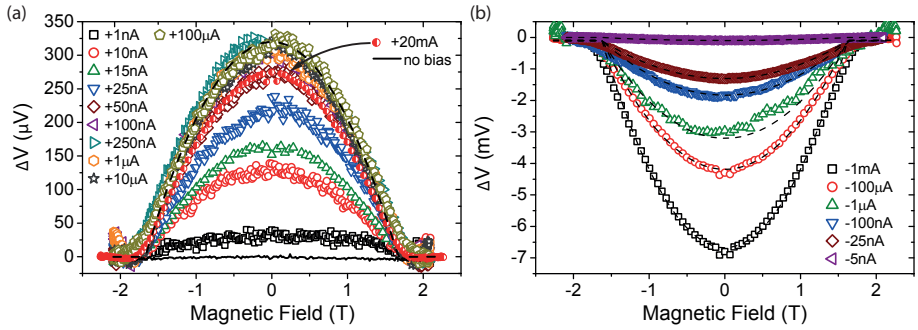

Figure 6.3: (a) Change in the junction voltage as function of the applied out-of-plane magnetic field for several current biases (open symbols), the background voltage has been subtracted. An increase in the amplitude is observed up to 50 nA after which it saturates for many order of magnitude of increase in current bias. At a very large bias of 20 mA the amplitude slightly decays. The solid black line is the response when zero current is sourced. (b) Similar as in (a) but for negative bias currents. Unlike for positive bias a continuous increase of the amplitude is observed with current bias up to −1 mA. The dash black lines in both graphs are fits as described in the text.

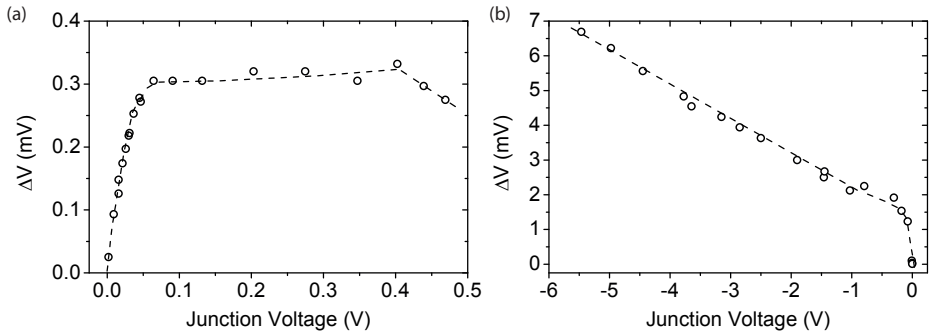

Figure 6.4: (a) Amplitude of the TAMR effect as a function of positive (forward biased) junction voltage. A very rapid increase in the TAMR effect is observed in the low voltage region after which the amplitude saturates, above 0.4 V the TAMR slightly decreases. (b)) Amplitude of the TAMR effect as a function of negative junction voltage. A very rapid increase in the TAMR amplitude is observed at low bias. At large negative voltage a linear scaling of the TAMR amplitude is observed unlike the forward biased case. Note that a much larger junction voltage can be developed at negative voltage since the Schottky junction is reversed biased.

amplitude at negative bias as well as the significantly smaller amplitude at positive polarity has been observed before in FM/n-GaAs junctions [2]. Note however that they did not observe the very rapid increase of the TAMR amplitude at low voltage.

The TAMR size is defined as the TAMR amplitude divided by the background

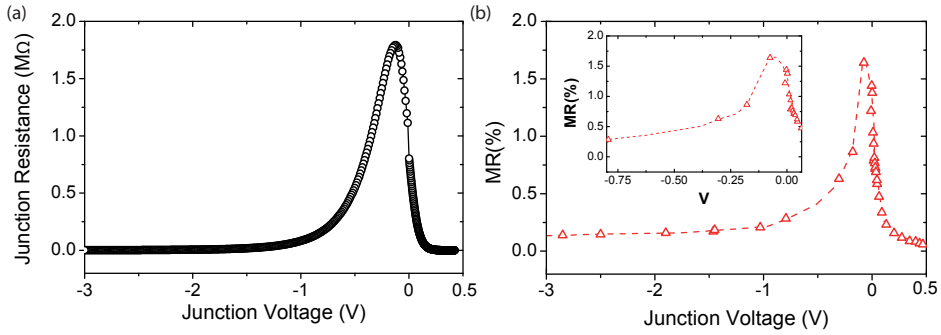

Figure 6.5: (a) Junction resistance as a function of the junction voltage. (b) TAMR amplitude in percentage as function of junction voltage, a large effect $> 1.5\,\%$ is observed at low forward and reverse bias. Interestingly, the TAMR effect does not show a monotonous decay as function of junction voltage but a maximum is observed around $-75\,\mathrm{mV}$. Note that the junction resistance shows a similar non-monotonous behavior.

voltage,

$$\mathrm{TAMR}\,(\%) = \frac{V(\theta = 0°) - V(\theta = 90°)}{V(\theta = 0°)} \tag{6.1}$$

In Fig. 6.5(b) the TAMR size is shown as a function of junction voltage. At low bias the TAMR amplitude is as large as 1.7 % and decays rapidly with increasing bias. The reduction is significantly faster in the forward bias direction (+V) compared to the reverse bias direction (-V), such behavior has also been observed for (Ga,Mn)As/N-GaAs Zener-Esaki diodes although at 4.2 K [20]. The inset shows however, that the TAMR size does not decay monotonously in the reverse bias direction but has a clear maximum around $-75\,\mathrm{mV}$. This is of great interest since the TAMR effect is generally seen to decay very rapidly when increasing bias in either direction [4, 8–10], resulting in a significant reduction of the TAMR effect at the junction voltages needed to operate practical devices. Apart from this the room temperature TAMR size ($\sim 1.7\,\%$) is much larger than commonly observed for transition metal ferromagnet based tunnel junction using either non-magnetic metals or GaAs as a counter electrode [1, 2, 5–8]. It is even much larger compared to anti-ferromagnetic (AFM) based TAMR devices using IrMn where at low temperature effects of 160 % where observed but TAMR vanished above 100K[11]. Later room temperature TAMR was achieved by a different group using Pt/Co multilayers in contact with AFM IrMn but a maximum effect of 0.24 % was observed [3] (for a more complete overview the reader is referred to table A.1 in the introduction).

The gross features of the TAMR amplitude with bias can be understood by considering the electron conduction through a biased Schottky junction. At forward bias the Schottky barrier is lowered resulting in a stronger contribution of thermionic emis-

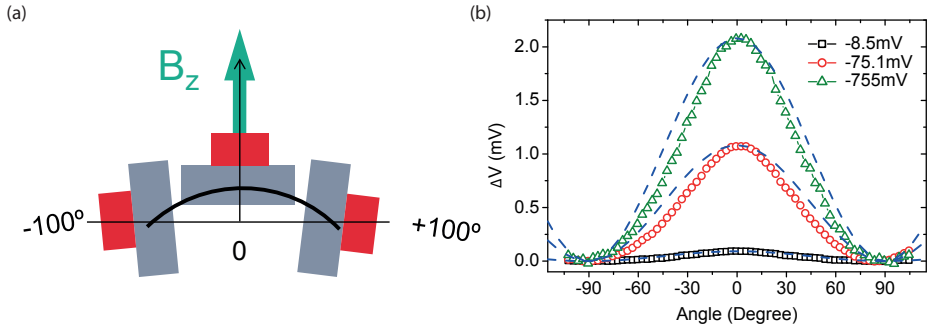

Figure 6.6: (a) Experimental setup to measure the angular dependence of the TAMR effect. A large magnetic field B_Z of 6 T is applied perpendicular to the surface normal. (b) Junction voltage as a function of sample angle with the applied magnetic field for different junction biases: −8.5 mV (black squares), −75.1 mV (red circles) and −755 mV (green triangles). A two fold symmetry is observed consistent with the TAMR effect, the blue dashed lines are fits using the expected angular dependence of the out-of-plane TAMR effect.

sion (non-tunneling transport). When applying a reverse bias the Schottky barrier is not lowered and the charge transport mainly consist of thermally excited electron which tunnel through the barrier. Hence a softer decay of the TAMR amplitude is expected when reverse biasing the Schottky junction. Even though tunneling transport dominates the charge transport at large negative bias a reduction in the TAMR effect is expected. This is because the tunnel spin polarization of the Co reduces when electrons are tunneling from a large distribution of states well below the Fermi level.

Another way to characterize the TAMR effect is by rotating the sample in a large, constant magnetic field as shown in Fig. 6.6(a). The field should be large such that it will fix the magnetization direction of the FM along the direction of the applied magnetic field. A field of 6 T is applied which is significantly larger than the 1.7 T needed to align the FM magnetization along the out-of-plane hard axis. When the sample is rotated this will fix the magnetization direction almost completely along the applied magnetic field in the z-direction. This effectively causes a gradual rotation of the magnetization with respect to the current direction and the interface surface normal. In this case a 2-fold symmetry is expected for out-of-plane TAMR with an angular dependence of $\cos(2\theta) + 1$ where the angle θ is defined as the angle of the magnetization with the surface normal as shown in Fig. 6.2 [21, 22]. In Fig. 6.6(b) such measurements are shown for three different junction voltages of −8.5 mV (black squares), −75.1 mV (red circles) and −755 mV (green triangles). The dashed blue lines are fits using the angular dependence $\cos(2\theta)+1$ and show good agreement although the measured TAMR lineshape is slightly more narrow. The good agreement with the expected angular dependence as well as the 2-fold symmetry are consistent with the out-of-plane TAMR effect. The slight deviation at intermediate angels might be

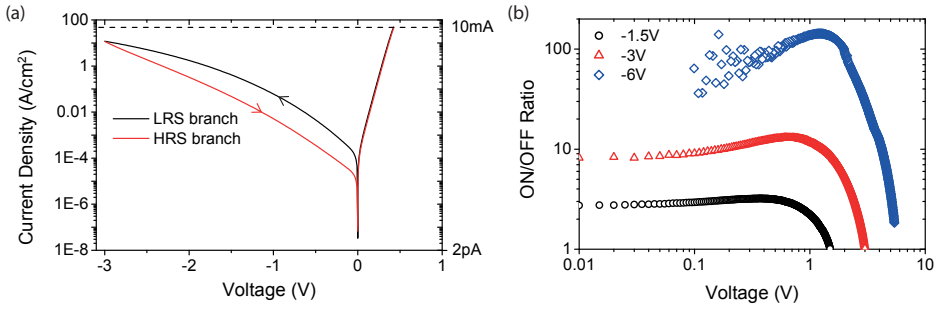

Figure 6.7: (a) Current-Voltage response of a Co/Nb:$SrTiO_3$ junction exhibiting electro-resistance. The device is reset to the HRS when sweeping from 430 mV to −3 V (black solid line), as can be observed when sweeping back from −3 V to zero (red solid line). The device is set to the LRS by sweeping the voltage from zero to 430 mV. (b) The electro-resistance is defined as the ratio of the current of the lower HRS branch divided by the upper LRS branch. A maximum ratio of ∼13 is observed when sweeping up to −3 V. When sweeping to −1.5 V (not shown in (a)) a maximum ratio of ∼3.2 is obtained.

caused by the the slight rotation of the magnetization when rotating the sample since even a 6 T field will not full fix the magnetization along the z-direction.

6.2.2 Electro-Resistive switching measurements

A typical hysteric *I-V* response of the same junction is shown in Fig. 6.7(a) where the voltage is swept from a positive voltage to −3 V (black curve) and back (red curve). A sweep rate of 50 mV s^{-1} is used. When sweeping from a positive to negative bias the device is in the LRS (upper branch of the *I-V*), and in the HRS when sweeping back (lower branch). To define the effect size the on/off ratio is plotted in Fig. 6.7(b) defined as the ratio of the HRS/LRS. In the figure the ratio is calculated for −6 V (blue diamonds), −3 V (red triangles) and −1.5 V (black circles) sweeps. The *I-V* for the −6 V and −1.5 V sweep are not shown. A maximum ratio of 150 at −1.2 V, 13 at −675 mV and 3.2 at −375 mV is found when sweeping to −6 V,−3 V and −1.5 V, respectively. A ratio of around 80 and 8 is seen at voltage small enough for read out purposes ($\leq$ 100 mV) for the −6 V and −3 V sweep.

Note that it is possible to obtain a different absolute resistance in the HRS state by sweeping to a larger/smaller negative voltage, resulting in a larger/smaller resistance at low voltage read-out (see Fig. 6.2). Also note that by employing the same set voltage the LRS is always the same and hence acts as a well defined reference resistance. The ability to set the device resistance to various values is of interest for realizing multi-state logic devices.

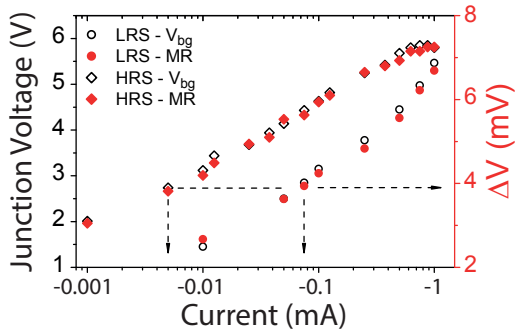

Figure 6.8: Background voltage and TAMR amplitude as function of current bias when the junction is set in the HRS (upper data sets) and LRS (lower data sets). The black open symbols refer to the left axis (junction voltage) and the solid red symbols to the left axis (TAMR amplitude). The TAMR amplitude is unaffected by the resistance state of the device as can be seen by following the dashed lines. The left dashed arrow points towards data in the HRS where a junction voltage of −2.7 V is obtained at a −5 µA bias, the corresponding TAMR amplitude is almost 4 mV. When the junction is set to the LRS a bias current of −75 µA is needed to reach a junction voltage of −2.7 V, despite the significantly larger current a TAMR amplitude of almost 4 mV is observed similar to the HRS amplitude. This correlation is seen for almost the full data set and shows that the TAMR amplitude is independent of the junction current, it only depends on the voltage drop at the interface.

6.2.3 Combined resistive switching and TAMR

To investigate the interplay between the resistive switching and the TAMR response a set of bias dependent TAMR measurements were performed in both a HRS and LRS state. The junction voltage and TAMR amplitude for different bias currents are shown in Fig. 6.8. Two different branches are visible, the upper set of data corresponds to the HRS (diamonds) and the lower one to the LRS (circles). The black open symbols correspond with the left axis and are the background voltages of the junction at a certain bias current. The solid red symbols correspond with the right axis and are the measured TAMR amplitudes.

That the upper data set corresponds to the HRS can be seen by comparing the background voltage at a certain bias. For instance at a current of −5 µA a background voltage of −2.7 V is generated (left dashed arrow). To obtain the same voltage in the LRS (follow the horizontal dashed line) a current of −75 µA needs to be sourced. Interestingly, the TAMR amplitude is almost exactly the same for both resistance states as long as the same background voltage is realized. This can be seen by following the dashed line all the way to the right axis. This relationship is maintained over a very large bias range which suggests that the TAMR amplitude does not depend on the current but only the voltage drop over the depletion region. Therefore, these devices

can be resistively switched without significantly effecting the spintronic properties. This is generally not possible for instance when the resistive switching is based on the formation of conducting filaments in a insulating material. In such cases the spintronic effect is coupled to the charge transport and filament formation either creates a GMR like memory by spin transport through the filament [23] or oppositely a TMR effect exists in the HRS where electrons tunnel through the oxide while in the LRS the formation of a conducting path removes the TMR effect [24].

6.3 Discussion

Compared to tunnel junctions exhibiting room temperature TAMR reported in the literature, the devices in this chapter show a significantly larger TAMR effect size as well as a relatively robust bias dependence at reverse bias. This enhancement can be, at least partly, explained by the large dielectric permittivity of n- $SrTiO_3$. Out-of-plane TAMR can emerge in tunnel junctions when a large enough Bychkov-Rashba Spin-Orbit Field (SOF) arises at the interface. Such a SOF arises in junctions where an electric field gradient exists. For the devices in this chapter the Schottky barrier provides such an electric field normal to the surface. For more details the reader is referred to section 2.2.9. In such a Schottky junction not only an electric field develops inside the depletion region of the semiconductor but an equal amount of charge, of opposite polarity, resides on the interfacial surface layer of the metal. This is referred to as the depletion charge and is equal to $Q_{\mathrm{dep}} = qN_{\mathrm{D}}W$ with W the depletion width, when assuming the full depletion approximation. For semiconductors with a constant permittivity it holds that $W \propto \sqrt{\epsilon_r}$. Hence for the same doping density (N_{D}) the depletion width is much larger for n-$SrTiO_3$ compared to for instance n-GaAs. This leads to a depletion charge in the n-$SrTiO_3$ device which is larger than n-GaAs given by $Q_{\mathrm{dep}}^{\mathrm{STO}}/Q_{\mathrm{dep}}^{\mathrm{GaAs}} = \sqrt{\epsilon_{\mathrm{STO}}/\epsilon_{\mathrm{GaAs}}} \approx 5$. Hence, a roughly 5 times larger charge is present on the cobalt surface in a Co/n-$SrTiO_3$ Schottky junction than a Co/n-GaAs. Since the Bychkov-Rashba SOC strength scales with the electric field size this results in an enhancement of the TAMR effect.

Additionally a much larger doping density can be used in n-$SrTiO_3$ Schottky junctions while still maintaining non-ohmic tunneling charge transport. For instance, the TAMR effect in CoFe or Fe/n-GaAs junctions is generally reported for a doping density of around 3 to 5×10^{18} cm^{-3} while in the current junctions the doping density is around 3 to 5×10^{19} cm^{-3}. This means that much larger Q_{dep} values can be obtained when utilizing n-$SrTiO_3$ junctions while still maintaining a wide enough depletion region to obtain, non-ohmic, tunneling transport. In the current devices the transport and depletion width of the devices are not tuned for maximizing the TAMR amplitude since there is for instance still a large thermal contribution to the tunneling transport. The ability to tune the depletion width using commercially available

Nb-doped $SrTiO_3$ substrates is limited due to the very restricted doping densities available. However, using hybrid MBE techniques it is possible to grow very high quality thin film doped $SrTiO_3$ layers which should allow precise control over the Schottky barrier profile such that device can be tuned into the pure tunneling regime [25]. This will create larger electric fields on the Co surface and can be expected to yield increased TAMR both due to the large electric field as well as predominant tunneling of electrons close the the Fermi level.

Note that while n-$SrTiO_3$ has a non-linear permittivity extremely large electric fields are needed to observe significant non-linear behavior at room temperature. The electric fields in the devices in this chapter are small enough that the non-linearity is small, hence the presented argumentation is valid at room temperature. To incorporate the non-linear behavior of n-$SrTiO_3$ the expressions for $W(E,T)$ as given in chapter 3 should be used.

An additional mechanism which could lead to enhancement of the TAMR effect size is the 3-d orbital nature of the n-$SrTiO_3$ conduction band. This leads to a better matching with the 3-d band of the Co electrode and can result in predominant tunneling via the 3-d states [26]. The 3-d states are more confined and have a larger SOC compared to the s or p states, normally dominant in the tunneling process. Combining inter-metallic AFM's such as IrMn, where the 5-d shell of Ir introduces significant SOC and the Mn 3-d shell has large magnetic moment, with the 3-d orbital derived conduction band of Nb:$SrTiO_3$ is expected to further increase room temperature TAMR.

Note that, in contrast with the results presented in chapter 4 where a 11 Å thick AlO_x barrier is inserted, it is not the SOF residing in the n-$SrTiO_3$ region but on the surface of Co that drives the large TAMR effect. Although this might seem puzzling, the insertion of a thin AlO_x layer significantly reduces the Schottky barrier height and depletion width and hence reduces Q_{dep} as discussed in chapter 3 and schematically shown in Fig. 6.9(a). Therefore, a much smaller electric field at the Co surface is present in the Co/AlO_x (11Å)/Nb:$SrTiO_3$ devices compared to the Co/Nb:$SrTiO_3$ Schottky junction. Additionally, the insertion of AlO_x electronically decouples the Co and n-$SrTiO_3$ 3-d states.

To investigate whether the insertion of a thin AlO_x layer indeed strongly suppresses the TAMR effect a device with an intermediate AlO_x barrier thickness of 7 Å is grown. Note that the electrical characteristics of this device are discussed in chapter 3.

6.3.1 Reduction of TAMR by insertion of ultra-thin tunnel barrier

The TAMR amplitude as function of junction voltage is shown in Fig. 6.9(b). Overall a very similar behavior is observed: a linear scaling of the TAMR amplitude at reverse bias (-V) is observed while the amplitude is much smaller at forward bias. Unlike the Schottky devices the TAMR effect strongly reduces at large enough forward bias, in

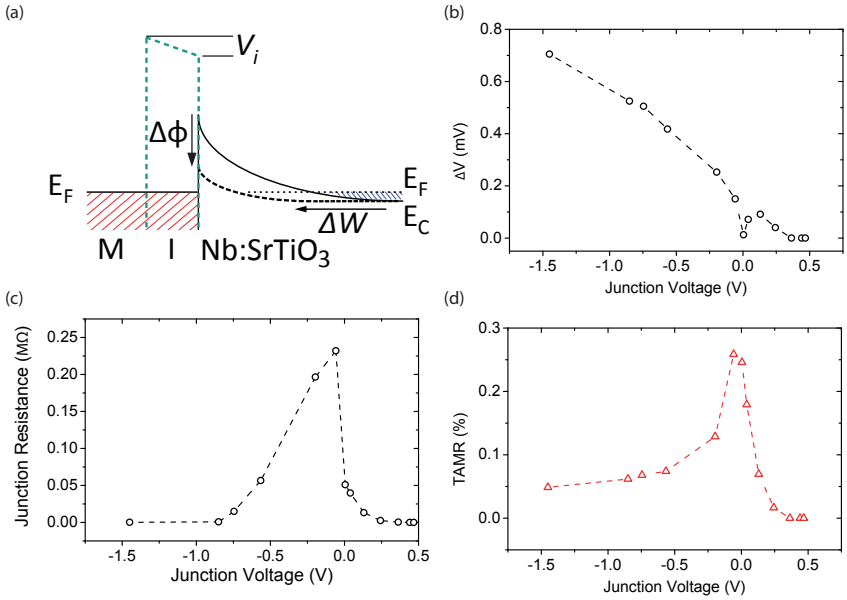

Figure 6.9: (a) Energy diagram of a FM/Nb:$SrTiO_3$ interface and the effect of insertion of a thin insulating tunnel barrier. The tunnel barrier causes a large reduction in the Schottky barrier height denoted by $\Delta\phi$ and the depletion region width denoted by ΔW. This significantly reduces the charge density on the metal surface and hence the electric field on the metal surface is largely reduced. (b) The bias dependence of the TAMR amplitude is similar to that observed for the Schottky junctions although smaller in magnitude (c) Junction resistance as function of junction voltage of a Co/AlO_x 7 Å/Nb:$SrTiO_3$ device (d) TAMR size as function of junction voltage of a Co/AlO_x 7 Å/Nb:$SrTiO_3$ device. A clear reduction of the TAMR size is observed compared to the Schottky devices. This is consistent within the framework of enhanced Rashba SOC at the Co surface due to the large permittivity of Nb:$SrTiO_3$.

this bias regime a Lorentzian like spin injection signal is observed similar to those observed in chapters 4 and 5 at large forward bias. The absolute size of the TAMR effect is significantly smaller than for the Schottky devices, for instance at −1.5 V a TAMR amplitude of around 0.7 mV is observed compared to 2.5 mV for the Schottky devices.

The reduction of the TAMR effect is clearly visible in Fig. 6.9(d) where the TAMR effect size is plotted as function of junction voltages. A maximum TAMR effect of 0.25 % is observed at low bias compared to more than 1.5 % for the Schottky devices. Note that the overall asymmetric decay of the TAMR size as function of voltage polarity is very similar to that observed for the Schottky junctions. The TAMR size and junction resistance also show a similar correlation as observed for the Schottky junctions in Fig. 6.5(a) and (b). Therefore it seems that indeed a TAMR effect of similar

origin is observed with a suppressed magnitude due to the insertion of a 7 Å thick AlO_x barrier.

6.4 Conclusions

Nb:$SrTiO_3$ Schottky junctions with Co contacts were fabricated and showed the coexistence of electro-resistive switching as well as a large TAMR effect at room temperature. Many devices on the same chip show very similar charge transport and TAMR effect behavior both qualitatively as quantitatively. The electro-resistance allows the junction to be used as a memory resistor when operated at low reverse bias while the TAMR effect is not significantly influenced by this process. The room temperature TAMR effect size is much larger than those reported in literature when using transition metal ferromagnets and has a unconventional bias dependence. The origin of this enhancement is explained by the large permittivity of n-$SrTiO_3$ and its Ti d-orbital derived conduction band.

A significant enhancement of the TAMR effects size is expected by optimizing the electro-static landscape of the devices, down scaling to smaller dimensions, fabricating single crystalline epitaxial ferromagnetic contacts or using heavy metal based FM or AFM's (such as IrMn, FeRh or FeMn). This can be realized relatively easily by better controlling the doping density of n-$SrTiO_3$, down scaling junction sizes via electron beam lithography and using different ferromagnetic contact material respectively. Additionally, it has recently been shown that the size and stability of the electro-resistive switching effects in such junction can be significantly enlarged and stabilized by defect engineering of the interfacial $SrTiO_3$ [18]. This shows considerable prospects for complex oxide based devices with combined spin and charge memory.

Acknowledgments

We would like to acknowledge J. G. Holstein, H. M. de Roosz, and H. Adema for the technical support.

References

[1] S. Hatanaka, S. Miwa, K. Matsuda, K. Nawaoka, K. Tanaka, H. Morishita, M. Goto, N. Mizuochi, T. Shinjo, and Y. Suzuki, "Tunnel anisotropic magnetoresistance in CoFeB/MgO/Ta junctions," *Appl. Phys. Lett.* **107**(8), 2015.

[2] C. Liu, Y. Boyko, C. C. Geppert, K. D. Christie, G. Stecklein, S. J. Patel, C. J. Palmstrm, and P. A. Crowell, "Electrical detection of ferromagnetic resonance in ferromagnet/n-GaAs heterostructures by tunneling anisotropic magnetoresistance," *Appl. Phys. Lett.* **105**(21), p. 212401, 2014.

[3] Y. Y. Wang, C. Song, B. Cui, G. Y. Wang, F. Zeng, and F. Pan, "Room-temperature perpendicular exchange coupling and tunneling anisotropic magnetoresistance in an antiferromagnet-based tunnel junction," *Phys. Rev. Lett.* **109**, p. 137201, Sep 2012.

[4] R. S. Liu, L. Michalak, C. M. Canali, L. Samuelson, and H. Pettersson, "Tunneling anisotropic magnetoresistance in $Co/AlO_x/Au$ tunnel junctions," *Nano Letters* **8**(3), pp. 848–852, 2008. PMID: 18254603.

[5] B. G. Park, J. Wunderlich, D. A. Williams, S. J. Joo, K. Y. Jung, K. H. Shin, K. Olejník, A. B. Shick, and T. Jungwirth, "Tunneling anisotropic magnetoresistance in multilayer-$(Co/Pt)/AlO_x/Pt$ structures," *Phys. Rev. Lett.* **100**, p. 087204, Feb 2008.

[6] J. Moser, A. Matos-Abiague, D. Schuh, W. Wegscheider, J. Fabian, and D. Weiss, "Tunneling anisotropic magnetoresistance and spin-orbit coupling in $Fe/GaAs/Au$ tunnel junctions," *Phys. Rev. Lett.* **99**, p. 056601, Aug 2007.

[7] L. Gao, X. Jiang, S.-H. Yang, J. D. Burton, E. Y. Tsymbal, and S. S. P. Parkin, "Bias voltage dependence of tunneling anisotropic magnetoresistance in magnetic tunnel junctions with MgOand Al_2O_3 tunnel barriers," *Phys. Rev. Lett.* **99**, p. 226602, Nov 2007.

[8] K. Wang, T. L. A. Tran, P. Brinks, J. G. M. Sanderink, T. Bolhuis, W. G. van der Wiel, and M. P. de Jong, "Tunneling anisotropic magnetoresistance in $Co/AlO_x/Al$ tunnel junctions with fcc Co (111) electrodes," *Phys. Rev. B* **88**, p. 054407, Aug 2013.

[9] T. Uemura, M. Harada, T. Akiho, K.-i. Matsuda, and M. Yamamoto, "Influence of GaAs surface structure on tunneling anisotropic magnetoresistance and magnetocrystalline anisotropy in epitaxial $Co_{50}Fe_{50}$/n-GaAs junctions," *Appl. Phys. Lett.* **98**(10), p. 102503, 2011.

[10] C. Rüster, C. Gould, T. Jungwirth, J. Sinova, G. M. Schott, R. Giraud, K. Brunner, G. Schmidt, and L. W. Molenkamp, "Very large tunneling anisotropic magnetoresistance of a $(Ga, Mn)As/GaAs/(Ga, Mn)As$ stack," *Phys. Rev. Lett.* **94**, p. 027203, Jan 2005.

[11] B. G. Park, J. Wunderlich, X. Martí, V. Holý, Y. Kurosaki, M. Yamada, H. Yamamoto, A. Nishide, H. Hayakawa, J.and Takahashi, A. B. Shick, and T. Jungwirth, "A spin-valve-like magnetoresistance of an antiferromagnet-based tunnel junction," *Nature Mater.* **10**, p. 347, 2011.

[12] T. Fujii, M. Kawasaki, A. Sawa, Y. Kawazoe, H. Akoh, and Y. Tokura, "Electrical properties and colossal electroresistance of heteroepitaxial $SrRuO_3/SrTi_{1-x}Nb_xO_3$ $(0.0002 \leqslant x \leqslant 0.02)$ schottky junctions," *Phys. Rev. B* **75**, p. 165101, Apr 2007.

[13] D. S. Shang, J. R. Sun, L. Shi, J. Wang, Z. H. Wang, and B. G. Shen, "Electronic transport and colossal electroresistance in $SrTio_3$:Nb-based Schottky junctions," *Applied Physics Letters* **94**(5), p. 052105, 2009.

[14] E. Lee, M. Gwon, D.-W. Kim, and H. Kim, "Resistance state-dependent barrier inhomogeneity and transport mechanisms in resistive-switching pt/srtio3 junctions," *Applied Physics Letters* **98**(13), p. 132905, 2011.

[15] D. Kan and Y. Shimakawa, "Transient behavior in Pt/Nb-doped $SrTiO_3$ Schottky junctions," *Appl. Phys. Lett.* **103**(14), p. 142910, 2013.

[16] M. Yang, L. Z. Ren, Y. J. Wang, F. M. Yu, M. Meng, W. Q. Zhou, S. X. Wu, and S. W. Li, "Direct evidences of filamentary resistive switching in pt/nb-doped srtio3 junctions," *Journal of Applied Physics* **115**(13), p. 134505, 2014.

[17] E. Mikheev, B. D. Hoskins, D. B. Strukov, and S. Stemmer, "Resistive switching and its suppression in $Pt/Nb:SrTiO_3$ junctions," *Nat. Commun.* **5**, June 2014.

[18] E. Mikheev, J. Hwang, A. P. Kajdos, A. J. Hauser, and S. Stemmer, "Tailoring resistive switching in

$Pt/SrTiO_3$ junctions by stoichiometry control," *Sci. Rep.* **5**, p. 11079, 2015.

[19] H.-S. Wong, H.-Y. Lee, S. Yu, Y.-S. Chen, Y. Wu, P.-S. Chen, B. Lee, F. Chen, and M.-J. Tsai, "MetalOxide RRAM," *Proceedings of the IEEE* **100**, pp. 1951–1970, June 2012.

[20] R. Giraud, M. Gryglas, L. Thevenard, A. Lemaître, and G. Faini, "Voltage-controlled tunneling anisotropic magnetoresistance of a ferromagnetic p^{++}-(Ga,Mn)As/n^{+}-GaAs Zener-Esaki diode," *Appl. Phys. Lett.* **87**(24), p. 242505, 2005.

[21] A. Matos-Abiague and J. Fabian, "Anisotropic tunneling magnetoresistance and tunneling anisotropic magnetoresistance: Spin-orbit coupling in magnetic tunnel junctions," *Phys. Rev. B* **79**, p. 155303, Apr 2009.

[22] A. Matos-Abiague, M. Gmitra, and J. Fabian, "Angular dependence of the tunneling anisotropic magnetoresistance in magnetic tunnel junctions," *Phys. Rev. B* **80**, p. 045312, Jul 2009.

[23] H.-J. Jang, O. A. Kirillov, O. D. Jurchescu, and C. A. Richter, "Spin transport in memristive devices," *Appl. Phys. Lett.* **100**(4), p. 043510, 2012.

[24] Q. Li, T.-T. Shen, Y.-L. Cao, K. Zhang, S.-S. Yan, Y.-F. Tian, , S.-S. Kang, M.-W. Zhao, Y.-Y. Dai, Y.-X. Chen, G.-L. Liu, L.-M. Mei, X.-L. Wang, and P. Grünberg, "Spin memristive magnetic tunnel junctions with CoO-ZnO nano composite barrier," *Sci. Rep.* **4**, p. 3835, 2014.

[25] J. Son, P. Moetakef, B. Jalan, O. Bierwagen, N. J. Wright, R. Engel-Herbert, and S. Stemmer, "Epitaxial $SrTiO_3$ films with electron mobilities exceeding 30,000 $cm^2v^{-1}s^{-1}$," *Nature Mater.* **9**, p. 482, 2010.

[26] J. P. Velev, K. D. Belashchenko, D. A. Stewart, M. van Schilfgaarde, S. S. Jaswal, and E. Y. Tsymbal, "Negative spin polarization and large tunneling magnetoresistance in epitaxial $Co/SrTiO_3/Co$ magnetic tunnel junctions," *Phys. Rev. Lett.* **95**, p. 216601, Nov 2005.